PAPER

Check for updates

Glycogen for Smyd3-antisense oligonucleotide delivery and enhanced liver cancer gene therapy

Ning Bai,[a] Yi Huang,[b] Jie Shen,[c] Yefan Peng,[d] Huijie Zhang [ID] *[ef] and Deqiang Hou*[a]

The overexpression of Smyd3 is closely related to the progression of various cancers. Smyd3 is overexpressed in liver cancers but is hardly detectable in normal tissues; consequently, it is attracting increasing attention as a target for liver cancer therapy. Therefore, silencing Smyd3 mRNA using antisense oligonucleotides (ASOs) offers a promising option for liver cancer therapy. However, their clinical application is hindered by their poor stability and cellular uptake. Although promising, strategies such as chemical modification of the ASOs as well as the synthetic nanocarriers raise safety concerns. The efficient delivery of ASOs into tumor cells remains a big challenge. In this study, we developed a novel glyco-nanovector for Smyd3-ASO delivery. Glycogen possesses an inherent dendritic nanostructure. Aminated glycogen (NG) was simply synthesized by grafting glycogen with diethylenetriamine (DETA). NG possessed good biocompatibility. Cationic NG efficiently formed a complex with Smyd3-ASOs and shielded them from enzymatic degradation. NG significantly enhanced the cellular uptake of Smyd3-ASOs in HepG2 cells. As a result, NG/ASOs decreased the translation of Smyd3 proteins from mRNA and thus inhibited the proliferation of HepG2 cells. This study underscores the potential of glycogen as an efficient nanovector for ASO delivery and cancer gene therapy.

1 Introduction

Globally, liver cancer remains one of the most prevalent malignancies and the third-highest cause of cancer-associated mortality.[1] Compared with the conventional therapeutic options, gene therapy has recently emerged as a promising alternative for liver cancer therapy due to its higher efficiency and minimal systemic cytotoxicity, especially for patients with advanced-stage liver cancer.[2] Gene therapy utilizes nucleic acid drugs to alter the expression of specific oncogenes, thereby achieving therapeutic effects. Among various nucleic acid drugs, antisense oligonucleotides (ASOs) are attracting increasing attention due to their precise targeting, straightforward design and low cost.[3] As single-stranded nucleic acids, ASOs bind to target RNA sequence *via* Watson–Crick base pairing to degrade, hinder or manipulate RNA.[4] To date, several ASO drugs have been approved by the FDA.[5] As a member of the Smyd family of lysine methyltransferases, Smyd-containing

protein 3 (Smyd3) overexpression is strongly associated with the proliferation, adhesion, invasion, and migration of cancer cells.[6–8] Smyd3 is overexpressed in liver cancers but is hardly detectable in normal tissues; consequently, it is attracting increasing attention as a target for liver cancer therapy.[9,10] Therefore, silencing Smyd3 mRNA using ASOs demonstrates great promise for liver cancer therapy. However, the clinical application of ASOs still faces significant hurdles due to rapid serum nuclease degradation and low penetrability.[3,11,12] Although encouraging, strategies such as chemical modification of the ASOs as well as viral vectors and synthetic nanovectors raise safety concerns.[3,13–18] Thus, a safer carrier capable of delivering ASOs into liver cancer cells is urgently needed.

Glycogen is a natural polysaccharide composed of repeating glucose units, which functions as the primary glucose reservoir in animal cells.[19] Glycogen exhibits an inherent dendritic nanostructure, which is beneficial for the encapsulation of drugs.[20–22] In addition, glycogen exhibits intrinsic non-toxicity and biodegradability; thus, it can be readily functionalized with various chemical groups.[20] These distinctive properties make glycogen an attractive vector for gene delivery.

This work presents a novel glyco-nanovector for the delivery of Smyd3-ASOs and enhanced liver cancer gene therapy (Scheme 1). Glycogen underwent covalent amination (NG) *via* grafting with diethylenetriamine (DETA). Then, the capacity of NG to encapsulate Smyd3-ASOs and shield them against nuclease degradation was examined. Thereafter, the cellular

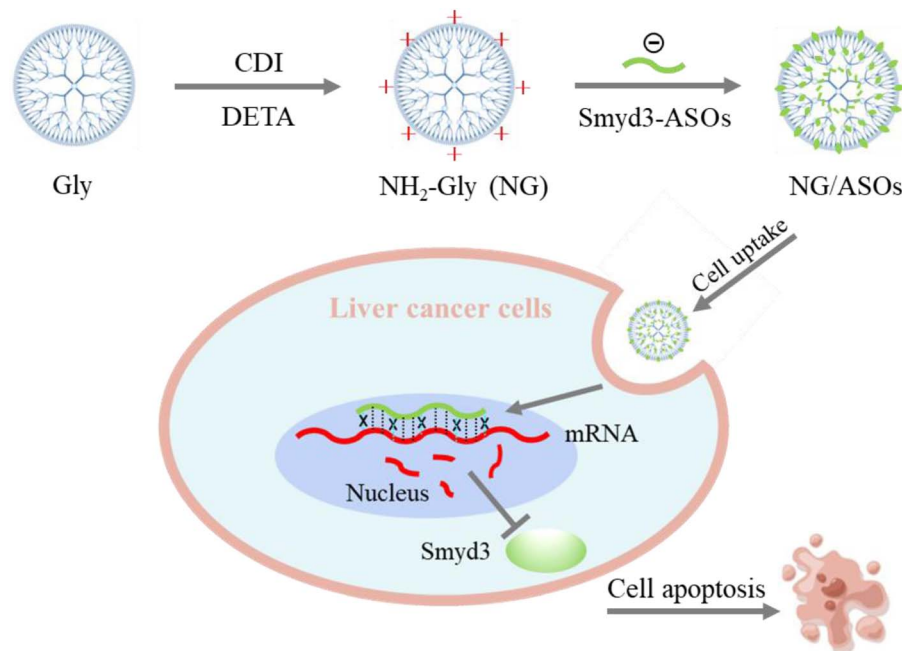*[a]Affiliated Hospital of Jiangnan University, Wuxi 214062, China. E-mail: Wan13114@163.com*

[b]Wuxi School of Medicine, Jiangnan University, Wuxi 214122, China

[c]Department of Anesthesiology, Jiangsu Institute of Nuclear Medicine Affiliated Jiangyuan Hospital, Wuxi 214000, China

[d]Innis College, University of Toronto, Toronto M5S1W7, Canada

[e]School of Life Sciences and Health Engineering, Jiangnan University, Wuxi 214122, China. E-mail: zhj0502@jiangnan.edu.cn; Fax: +86-510-85911900; Tel: +86-510-85911900

[f]Yunnan Baiyao Group Wuxi Pharmaceutical Co., Ltd, Wuxi 214028, China

Scheme 1 Scheme of the preparation of NG for Smyd3-ASO delivery and enhanced liver cancer gene therapy.

internalization of NG/ASOs was evaluated. Finally, the anti-tumor activity of the NG/ASOs against liver cancer cells was evaluated. We postulate that NG could facilitate the cellular internalization of Smyd3-ASOs due to its distinctive features. Therefore, NG/ASOs will effectively inhibit the proliferation of HepG2 cells by inducing apoptosis. Our findings underscore the potential of glycogen-based ASO delivery systems for liver cancer gene therapy.

2 Materials and methods

2.1 Reagents

Glycogen was obtained from Yuanye Biotechnology Co., Ltd (Shanghai, China). N,N'-carbonyldiimidazole (CDI) and diethylenetriamine (DETA) were purchased from Sinopharm Chemical Reagent Co., Ltd (Shanghai, China). N-Hydroxysuccinimide (NHS) and 1-(3-dimethylaminopropyl)-3-ethylcarbodiimide hydrochloride (EDC HCl) were obtained from Aladdin Reagent Co., Ltd (Shanghai, China). Smyd3-ASOs (5′-CGT ATT AAC ACT GGC A-3′) and FAM-labeled Smyd3-ASOs were purchased from Sangon Biotechnology Inc (Shanghai, China).

2.2 Synthesis of aminated glycogen (NG)

Aminated glycogen (NG) was synthesized *via* a two-step CDI-mediated coupling protocol.[20] Glycogen (400 mg) and CDI (400 mg) were suspended in 10 mL of DMSO. The solution was then stirred continuously for 2 hours under a nitrogen atmosphere. Afterwards, 1 mL of DETA was introduced into the solution, and the resulting mixture was stirred for an additional 24 hours. Finally, the mixture underwent dialysis for 3 days and was subsequently lyophilized to yield the NG.

2.3 Instrumentation

FTIR spectra were acquired using a TENSOR II spectrophotometer (Bruker, Germany). The ^{1}H NMR spectra were recorded on a 400 MHz AVANCE III spectrometer using D_2O as the solvent (Bruker, Germany). TEM images were captured with a JEM-2100 TEM (JEOL, Japan). UV-vis absorption spectra were obtained using a UV-2550 spectrophotometer (Shimadzu, Japan). DLS and zeta potential measurements were performed utilizing a Zetasizer Nano ZS instrument (Malvern, UK).

2.4 Cell culture

Mouse embryonic fibroblast cells NIH 3T3 and Human hepatocellular carcinoma cell line HepG2 were obtained from the Cell Bank of Chinese Academy of Sciences (Shanghai, China). The cells were cultured in DMEM with 10% FBS and maintained at 37 °C with 5% CO_2.

2.5 *In vitro* cytotoxicity assay

NIH 3T3 and HepG2 cells were seeded in 96-well plates (5000 cells/well). Following a 24 hours incubation period, NG in different concentrations (0–100 μg mL^{-1}) was added to the medium. After an additional 24 hours exposure, the cells were gently rinsed with PBS and subsequently incubated with 100 μL of MTT for another 4 hours. The medium was then aspirated and replaced with 100 μL of DMSO and incubated for 10 min at 37 °C. Finally, the absorbance at 570 nm was measured to quantify cell viability and assess the cytotoxic effect.

2.6 Hemolysis assay

The hemolysis analysis of NG was conducted following a previously reported method. PBS and deionized water were employed

as the negative control and the positive control, respectively. The hemolysis rate of NG in the presence of mouse red blood cells (RBCs) was calculated by the following formula:

$$\text{Hemolysis rate} = \frac{A_{\text{sample}} - A_{\text{PBS}}}{A_{\text{water}} - A_{\text{PBS}}} \times 100\%, \quad \text{where} \quad A_{\text{sample}}, \quad A_{\text{PBS}}$$

and A_{water} are the absorbance of the supernatant at 540 nm of the sample, PBS and water, respectively.

2.7 Preparation and characterization of NG/ASOs

The ASO solution was mixed with an NG solution in equal volumes at different weight ratios (1 : 1–1 : 8). Following a 1 hour incubation period, the mixture underwent centrifugation and washing steps to afford the NG/ASOs. The concentration of the unbound ASOs in the supernatant was determined using a spectrophotometer. The encapsulation efficiency (EE) was calculated by the following formula:

$$\text{EE} = \frac{C_{\text{initial}} - C_{\text{supernatant}}}{C_{\text{initial}}} \times 100\%, \quad \text{where} \quad \text{"}C_{\text{initial}}\text{"} \quad \text{and}$$

$C_{\text{supernatant}}$ are the initial concentration of ASOs and the concentration of unbound ASOs in the supernatant, respectively.

2.8 Agarose gel electrophoresis

Samples were loaded onto 2% agarose gel and subjected to electrophoresis at 80 mV for 25 min. The gels were visualized and captured using a GelDoc XR System (Biorad, USA).

2.9 Stability of NG/ASOs

Naked ASOs and NG/ASOs were treated with a DNase I solution for varying durations. Following enzymatic digestion, 1.25 μL of 50 mM EDTA was added to each sample to inactivate the DNase I activity. Then, the products were subjected to agarose gel electrophoresis.

2.10 Cell imaging

HepG2 cells (5×10^4) were inoculated in confocal dishes and incubated overnight. Subsequently, FAM-labeled samples were added to the medium, and the cells were incubated for 4 hours. Thereafter, cells were washed with PBS and then fixed with 3.7% (v/v) paraformaldehyde. Nuclear staining was performed using DAPI (Beyotime, China). The cells were visualized using a C2 Plus confocal laser scanning microscope (Nikon, Japan).

2.11 Flow cytometry analysis

HepG2 cells (1.5×10^5) were seeded into 6-well plates and cultured overnight. FAM-labeled samples were subsequently added to the medium, followed by a 4 hours incubation. Then, the medium was aspirated, and the cells were washed and collected by centrifugation. Cellular uptake was quantified using a CytoFLEX flow cytometer (Beckman Coulter, USA).

2.12 *In vitro* antitumor effect of NG/ASOs

For the MTT assay, HepG2 cells were inoculated in 96-well plates (5000 cells/well) and incubated for 24 h. Subsequently, NG/ASOs at varying ASO concentrations (0–50 μg mL^{-1}) were

introduced into the well. Following a 24 hours incubation period, the cells were rinsed with PBS and subsequently incubated with 100 μL of MTT solution for an additional 4 hours. Then, the medium was aspirated and replaced with 100 μL of DMSO, and the plate was incubated for 10 min at 37 °C. Finally, the absorbance at 570 nm was measured to evaluate the cell viability and anti-proliferative effect of NG/ASOs.

For the live/dead cell viability assay, HepG2 cells (2×10^5) were inoculated in 24-well plates and incubated overnight. Then, samples were added to the dish. After 24 h, the cells were rinsed with PBS and then incubated with a Calcein-AM/PI staining solution for 30 min. Subsequently, the staining solution was removed, and the cells were visualized by CLSM.

For the cell apoptosis assay, HepG2 cells (2×10^5) were seeded into 6-well plates and cultured overnight. The cells were then treated with test samples for an additional 24 hours, followed by staining with Annexin V-FITC/PI solution. Apoptotic and necrotic cells were subsequently analyzed by flow cytometry.

2.13 Statistical analysis

Experiments were conducted in triplicate. Statistical analysis was performed using Student's *t*-test. Data were expressed as mean ± standard deviation.

3 Results and discussion

3.1 Preparation and characterization of aminated glycogen (NG)

Aminated glycogen (NG) was synthesized following a previously reported method (Fig. 1).[20] DETA was conjugated to the hydroxyl group of glycogen through an amide bond. The obtained product was characterized by FTIR and ^{1}H NMR spectra. After amination, glycogen revealed new absorption bands at 1690 cm^{-1} (amide I band), 1540 cm^{-1} (bending vibration of –NH$_2$) and 1267 cm^{-1} (C–N stretching vibration), respectively, confirming the successful synthesis of NG (Fig. 2a).[20,23] This result suggested the successful synthesis of NG. The ^{1}H NMR spectrum of NG exhibited new broad peaks between 2.8 and 3.2 ppm, corresponding to the CH$_2$ group in DETA (Fig. 2b). The amination resulted in a surface charge reversal of glycogen from −9.4 mV to +27.3 mV, which facilitate the electrostatic complexation with ASOs and promote their cellular internalization (Fig. 2c). Subsequent TEM analysis revealed that NG exhibited well-dispersed spherical structures with sizes of about 60 nm (Fig. 2d). This finding was further corroborated by DLS analysis. NG exhibited a homogeneous size distribution in PBS (Fig. 2e).

3.2 Biocompatibility of NG

The biocompatibility of NG was assessed through *in vitro* cytotoxicity and blood compatibility assay. NIH 3T3 cells were used as the normal cell model. NG exposure at elevated concentrations did not induce significant proliferative inhibition in NIH 3T3 or HepG2 cells, as evidenced by the MTT assay (Fig. 3a). This result suggested that NG exhibited excellent
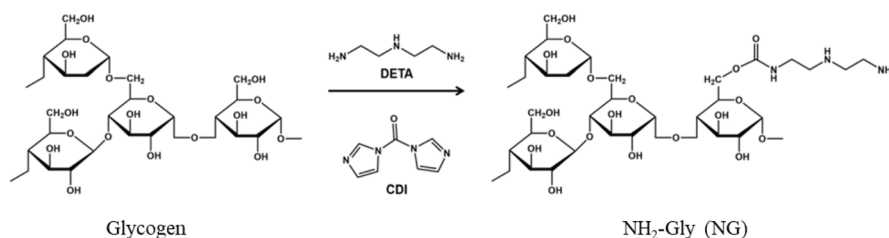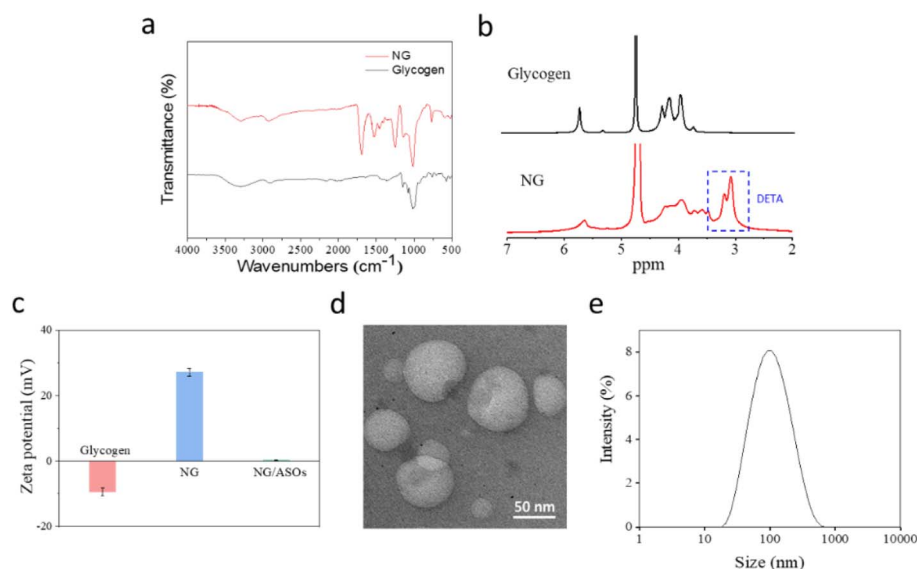
Fig. 1 Synthetic route of NG.

Fig. 2 Characterizations of NG. (a) FTIR spectra. (b) ^1H NMR spectrum. (c) Zeta potential. (d) TEM image. (e) Size distribution.

cytocompatibility. The hemolytic potential of NG was further assessed *via* a standardized hemolysis assay. NG at all tested concentrations yielded hemolysis ratios below 2%, significantly lower than the FDA-recommended threshold of 5% for biomaterials (Fig. 3b). Digital imaging analysis revealed that NG induced negligible hemoglobin release even at high concentrations. These results suggested that NG possesses good blood compatibility.

3.3 Preparation and characterization of NG/ASOs

NG encapsulated negatively charged ASOs mainly through electrostatic interactions, as evidenced by the reduction in the zeta potential (Fig. 2c). The peak corresponding to ASOs (260 nm) was also observed in the UV-vis absorption spectra of NG/ASOs, suggesting the successful complexation of ASOs by NG (Fig. 4a). Subsequently, a gel retardation assay was conducted to
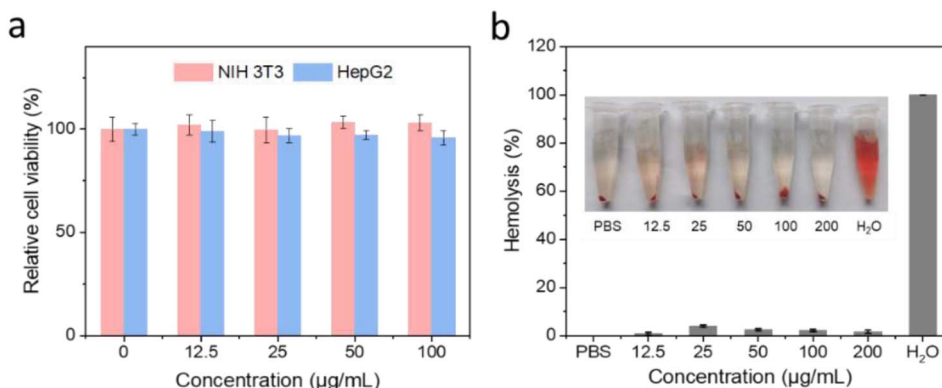

Fig. 3 Biocompatibility of NG. Relative cell viability of NIH 3T3 and HepG2 cells incubated with NG. (c) Hemolysis of RBCs following incubation with NG.
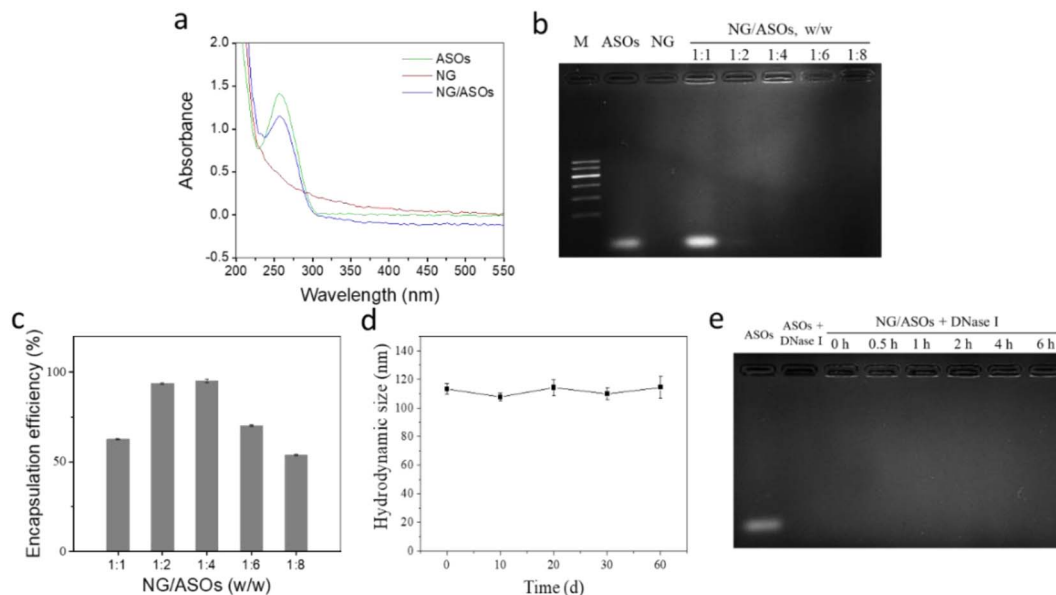
Fig. 4 Characterizations of NG/ASOs. (a) UV-vis absorption spectra. (b) Agarose gel electrophoresis. (c) Encapsulation efficiency. (d) Aqueous stability of NG/ASOs with respect to hydrodynamic diameter in PBS. (e) Gel electrophoresis of ASOs and NG/ASOs pre- and post-DNase I digestion.

study the loading behavior of the ASOs on NG (Fig. 4b). Naked ASOs appeared noticeably at the bottom of the lane. In contrast, upon complexation with NG, the ASOs lost mobility and were gradually trapped in the gel wells during electrophoresis, providing evidence for the formation of NG/ASOs complexes. A high encapsulation efficiency of about 95.2% was achieved
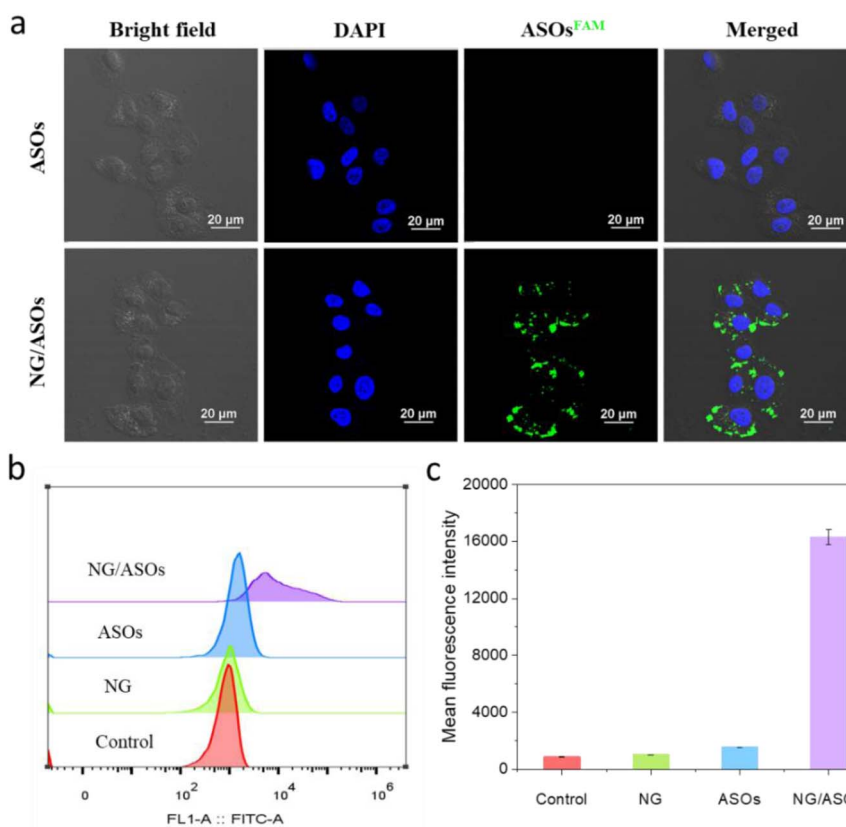

Fig. 5 Cellular uptake of NG/ASOs. (a) CLSM images of HepG2 cells following 4 hours incubation with different ASO samples. Cell nuclei were stained with DAPI (blue). FAM-labeled ASOs (green). The final concentration of NG was 15 μg mL^{-1}. (b) Flow cytometric analysis of HepG2 cells exposed to various ASO formulations. (c) MFI values of the flow cytometry-analyzed sample. Scale bar: 20 μm.

Paper

RSC Advances

when the weight ratio (NG/ASOs) was 1 : 4, and this ratio was utilized in the subsequent experiment (Fig. 4c). The hydrodynamic size of the NG/ASOs remained about 120 nm even when the solution was statically placed for 30 d (Fig. 4d). This result indicated that NG/ASOs possessed good aqueous stability.

To address the challenge of ASO instability in biological fluids, we evaluated the nuclease resistance of NG/ASO. The band of naked ASOs vanished following 30 minutes DNase I treatment, demonstrating the complete enzymatic degradation of naked ASOs by DNase I (Fig. 4e). In contrast, bands of NG/ASOs remained clearly visible after nuclease digestion. We further quantitatively analyzed the densitometry of the NG/ASO bands using ImageJ software. Following a 6 hours nuclease digestion, the band densitometry (0.066) remained largely comparable to that of the untreated sample (0.069). Therefore, NG shielded the ASOs from enzymatic degradation.

3.4 Cellular uptake of NG/ASOs

The cellular uptake of ASOs is crucial for their therapeutic activity. Thus, we investigated the cellular uptake of NG/ASOs using CLSM. The naked ASO group exhibited almost no green fluorescence, suggesting poor cellular internalization without a carrier (Fig. 5a). In contrast, cells cultured with NG/ASOs exhibited obvious fluorescence. This result demonstrated that NG markedly promoted the cellular uptake of ASOs.

The enhanced cellular uptake of ASOs was further validated using a flow cytometer. The NG/ASOs possessed the highest fluorescence intensity (Fig. 5b and c). As we know, the naked ASOs exhibited high susceptibility to enzymatic degradation. In contrast, NG/ASOs demonstrated superior serum stability due

to the protective effect of NG. Furthermore, the naked ASOs could not easily penetrate cell membranes *via* only passive diffusion due to electrostatic repulsion, which resulted in limited cellular uptake. Owing to its inherent nanosize and spherical structure, glycogen is predisposed to caveolae-mediated endocytosis. Moreover, cationic NG would facilitate clathrin-mediated endocytosis by enabling strong interactions with negatively charged proteoglycans on the cell membrane. Therefore, nanoscale NG/ASO complexes could be efficiently internalized through multiple endocytic pathways, including clathrin and/or caveolae-mediated endocytosis.

3.5 *In vitro* antitumor evaluation

MTT assay was initially conducted to assess the antitumor effect of NG/ASOs on HepG2 cells. As shown in Fig. 6a, the naked ASOs showed a weak inhibitory effect on the proliferation of HepG2 cells due to their poor cellular uptake. In contrast, the NG/ASOs exhibited concentration-dependent anti-proliferative effects on HepG2 cells. This result suggested that a high amount of ASOs was delivered into the HepG2 cells by NG. The internalized ASOs are further bound to Smyd3 mRNA and suppress its expression in tumor cells through antisense, thereby promoting the apoptosis of HepG2 cells.

The live/dead cell double-staining assay further confirmed the enhanced antitumor effect of NG/ASOs against HepG2 cells. As shown in Fig. 6b, live cells were labeled with green fluorescence, whereas dead cells exhibited a red color. Compared with the control and naked ASO groups, NG/ASOs caused the most cell death and significantly decreased the cell viability. This result was also in accordance with flow cytometry analysis. As
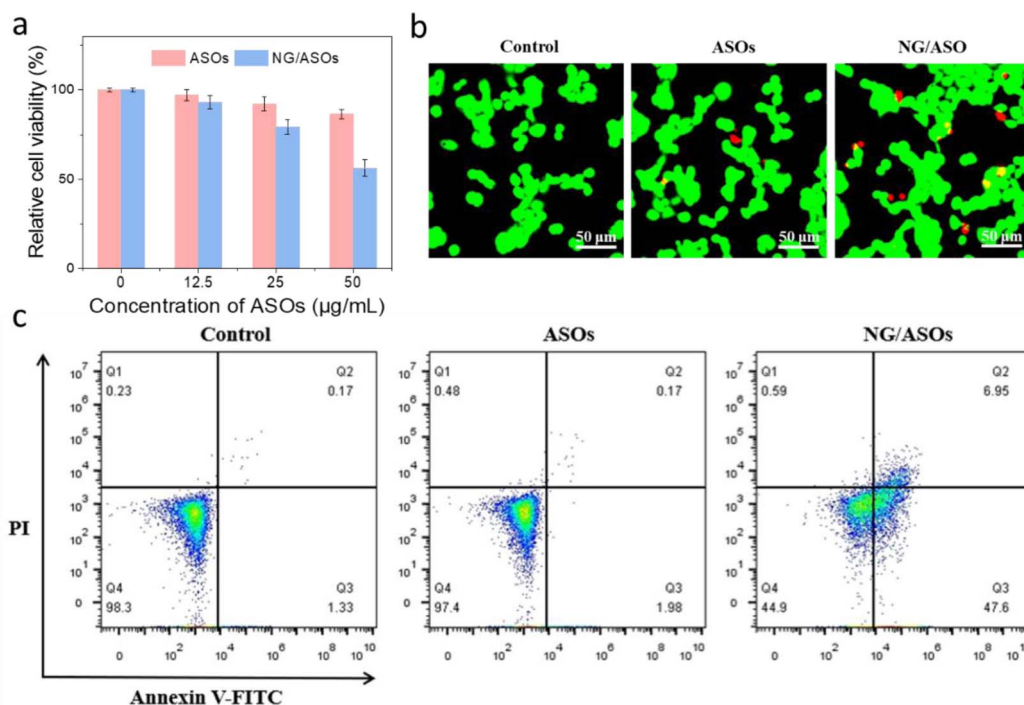

Fig. 6 Antitumor activity of NG/ASOs against HepG2 cells. (a) MTT assay. (b) Live/dead cell double-staining assay. (c) Flow cytometry analysis of the cell apoptosis. Scale bar: 50 μm.

shown in Fig. 6c, the apoptosis rate of the NG/ASO group (54.55%) was much higher than that of the naked ASO group (2.15%). Taken together, NG/ASOs notably inhibited the proliferation of HepG2 cells and effectively promoted their apoptosis. Although the *in vitro* results are promising, further *in vivo* experiments are still needed before making a definitive conclusion about their antitumor effects, which are also essential for the practical application of NG/ASOs in cancer gene therapy.

4 Conclusion

In summary, we constructed a novel Smyd3-ASO delivery system for enhancing the efficacy of liver cancer gene therapy. NG was readily synthesized by grafting DETA onto glycogen. The dendritic structure and cationic surface properties of NG enabled the efficient encapsulation of Smyd3-ASOs and shielded them against enzymatic degradation. Owing to the unique dendritic structure and positive surface charge, NG encapsulated Smyd3-ASO well and protected them from nuclease digestion. NG significantly enhanced the cellular uptake of Smyd3-ASOs in HepG2 cells. Therefore, NG/ASOs effectively inhibited the proliferation of HepG2 cells by inducing apoptosis. Our work underscores the potential of NG as an efficient and secure nano-vector for liver cancer gene therapy.

Author contributions

Ning Bai: investigation, methodology, formal analysis, data curation, writing – original draft. Yi Huang: investigation, methodology, formal analysis, data curation. Jie Shen: investigation, methodology. Yefan Peng: formal analysis, data curation. Huijie Zhang: project administration, conceptualization, validation, writing – original draft, writing – review & editing, funding acquisition. Deqiang Hou: project administration, conceptualization, writing – review & editing, funding acquisition.

Conflicts of interest

There are no conflicts to declare.

Data availability

The data that support the findings of this study are available from the corresponding author upon reasonable request.

Acknowledgements

References

1 K. E. R. Bowman, P. Lu, E. R. Vander Mause and C. S. Lim, *Ther. Delivery*, 2020, **11**, 833–850.

2 K. Kamimura, T. Yokoo, H. Abe and S. Terai, *Cancers*, 2019, **11**, 1865.

3 T. Ramasamy, H. B. Ruttala, S. Munusamy, N. Chakraborty and J. O. Kim, *J. Controlled Release*, 2022, **352**, 861–878.

4 S. T. Crooke, X. H. Liang, B. F. Baker and R. M. Crooke, *J. Biol. Chem.*, 2021, **296**, 100416.

5 D. Collotta, I. Bertocchi, E. Chiapello and M. Collino, *Front. Pharmacol*, 2023, **14**, 1304342.

6 Z. Y. Zhou, H. Jiang, K. S. Tu, W. Yu, J. L. Zhang, Z. G. Hu, H. Y. Zhang, D. K. Hao, P. B. Huang, J. Wang, A. J. Wang, Z. Y. Xiao and C. C. He, *J. Exp. Clin. Cancer Res.*, 2019, **38**, 18.

7 M. T. Binh, N. X. Hoan, D. P. Giang, H. V. Tong, C. T. Bock, H. Wedemeyer, N. L. Toan, M. H. Bang, P. G. Kremsner, C. G. Meyer, L. H. Song and T. P. Velavan, *Sci. Rep.*, 2020, **10**, 346.

8 A. Giakountis, P. Moulos, M. E. Sarris, P. Hatzis and I. Talianidis, *Semin. Cancer Biol.*, 2017, **42**, 70–80.

9 H. Kontaki, M. Koukaki, M. Vasilarou, A. Giakountis, E. Deligianni, X. L. Luo, Y. Kim and I. Talianidis, *iScience*, 2021, **24**, 102473.

10 H. Y. Zhang, Z. Y. Zheng, R. Q. Zhang, Y. C. Yan, Y. R. Peng, H. Ye, L. H. Lin, J. Y. Xu, W. B. Li and P. B. Huang, *Cell Death Dis.*, 2021, **12**, 1097–1154.

11 Y. Chen, Z. K. Guo, J. Li, K. M. Wang and J. Huang, *Coord. Chem. Rev.*, 2025, **535**, 216673.

12 M. Gagliardi and A. T. Ashizawa, *Biomedicines*, 2021, **9**, 433.

13 H. W. Liao, S. Y. Wang, X. N. Wang, D. Z. Dai, Y. Zhang, C. H. Zhu and J. B. Li, *Chem. Biomed. Imaging*, 2024, **2**, 313–330.

14 X. H. Ye, S. H. Chen, W. Xiong, F. Wang, H. F. Chan, H. C. Lai, X. Y. Guo, T. T. Yang, S. H. Shen, H. Chen, W. X. Wang, G. S. Liu, Y. L. Guo and J. S. Chen, *Adv. Sci.*, 2025, **12**, 2417363.

15 L. J. Zhou, J. Bi, S. H. Chang, Z. S. Bai, J. Q. Yu, R. R. Wang, Z. H. Li, X. Zhang, J. J. Chou and L. Q. Pan, *Angew. Chem., Int. Ed.*, 2025, **64**, e202415272.

16 M. Egli and M. Manoharan, *Nucleic Acids Res.*, 2023, **51**, 2529–2573.

17 T. C. Roberts, R. Langer and M. J. A. Wood, *Nat. Rev. Drug Discovery*, 2020, **19**, 673–694.

18 D. Engelhardt, P. Nordberg, L. Knerr and L. R. Malins, *Angew. Chem., Int. Ed.*, 2024, **63**, e202409440.

19 M. Wojnilowicz, Q. A. Besford, Y.-L. Wu, X. J. Loh, J. A. Braunger, A. Glab, C. Cortez-Jugo, F. Caruso and F. Cavalieri, *Biomaterials*, 2018, **176**, 34–49.

20 H. J. Zhang, L. Lai, Z. Q. Wang, J. W. Zhang, J. Z. Zhou, Y. Nie and J. H. Chen, *Int. J. Biol. Macromol.*, 2024, **257**, 128536.

21 S. Fernandes, M. Quattrociocchi, M. Cassani, G. Savazzi, D. Johnson, G. Forte, F. Caruso and F. Cavalieri, *ACS Nano*, 2024, **18**, 28910–28923.

22 H. J. Zhang, K. K. Ma, H. Q. Liu, S. Wang, Z. Q. Wang, J. W. Zhang and J. H. Chen, *ACS Appl. Nano Mater.*, 2023, **6**, 22480–22487.

23 X. Liang, X. Ren, Z. Liu, Y. Liu, J. Wang, J. Wang, L.-M. Zhang, D. Y. B. Deng, D. Quan and L. Yang, *Int. J. Nanomed.*, 2014, **9**, 419–435.